Dipolar interactions between unpaired Si bonds at the (111)Si/SiO$_2$ interface

A. Stesmans and B. Nouwen*

Department of Physics, University of Leuven, 3001 Leuven, Belgium
(Received 24 August 1999; revised manuscript received 23 December 1999)

An electron spin resonance (ESR) study has been carried out on the P_b centers (interfacial $\cdot$Si$\equiv$Si$_3$) in standard thermal (111)Si/SiO$_2$, of which, in the as-grown state, a density 4.9×10^{12} cm^{-2} is inherently incorporated. The P_b density was significantly enhanced to various levels through post oxidation annealing in H$_2$ ambient at elevated temperatures. This resulted in the observation of distinct P_b density-dependent magnetic field angle anisotropy in the ESR spectra, herewith definitely establishing the importance of the magnetic dipolar interactions within the two-dimensional P_b defect system. Field angle dependence of dipolar origin is observed in linewidth, line shape, and resonance position. The data are interpreted within the framework of a computational model based on the magnetostatic approximation of the local magnetic field, which resulted in a detailed analysis of the line broadening mechanisms. The successful simulation provides evidence for P_b density-dependent variations in the strain broadening contribution, indicating a growing relaxation of the interfacial strain with increasing P_b density. Additionally, the spatial P_b defect distribution is found to exhibit a self-avoiding behavior, with apparently no P_b pairs occurring within third nearest-neighbor distance. These results are interpreted within a picture connecting defect generation with relaxation of interfacial strain. Magnetic susceptibility measurements reveal an almost purely Curie-type behavior of the P_b system with Curie temperature $T_c<1.3\pm0.8$ K.

I. INTRODUCTION

Thermal oxidation of Si is accompanied by the natural generation of dangling bond defects at the planar Si/SiO$_2$ interface as a result of lattice-network mismatch. Some types of these coordination point defects may be detected by electron spin resonance (ESR). In standard thermal (111)Si/SiO$_2$, the dominant defect observed by ESR is the P_b center, of which, in the as grown state, a density $N_0 \sim 4.9\times10^{12}$ cm^{-2} is inherently incorporated[1] for the oxidation temperature range 300–950 °C. Importantly, the P_b density was shown to be correlated with the average interface stress, which remains constant at the intrinsic mismatch related value throughout that oxidation temperature range. The defect has been conclusively identified[2,3] as an $sp^3_{[111]}$ dangling hybrid on an interfacial Si atom, backbonded to three Si atoms in the bulk, denoted as $\cdot$Si$\equiv$Si$_3$. Its thermochemical properties appear to be dominated by reversible passivation/depassivation interactions with hydrogen: It was demonstrated[2,4] that bonding to hydrogen transforms the P_b defect into a diamagnetic state, symbolized as P_bH. Recently, however, it has been found[5] that by appropriate post oxidation annealing (POA) in vacuum, substantial additional amounts of P_b defects can be created irreversibly (e.g., up to 7.5×10^{12} cm^{-2} at ~950 °C). The effect is strongly enhanced ($\sim6\times$) when performed in H$_2$. The creation mechanism thus allows one to achieve densities up to 3.1×10^{13} cm^{-2}, the maximum density ever reported.[5]

In contrast to the well-understood individual model of the P_b defect, little is known about the collective role P_b centers play in the overall interface structure. To this matter, information on the in-plane distribution of the defects would be useful. In principle, such information could be extracted from a detailed study of the magnetic dipolar interaction between the P_b defects at this essentially two-dimensional (2D) Si/SiO$_2$ interface. The 2D arrangement of the P_b system would give rise to anisotropic effects in the ESR spectra, which may offer a key to this information.

There has been some previous work on this matter. In a first work,[6] the P_b ESR linewidth and line shape was calculated using the classic method of moments, which had previously been successfully applied for a 3D spin system.[7] However, the method was eventually proven inadequate for the 2D case.[6,8–10] Instead, the dipolar effects on the P_b ESR linewidth and shape were then calculated using a computational model based on the exact solution of the Hamiltonian.[8] However, the effects were found not observable for the studied density $[P_b]\sim N_0$.[8] Later, though limited to the case with the applied magnetic field $\vec{B}\perp(111)$Si/SiO$_2$ interface, the first direct experimental evidence of dipolar interaction between P_bs was provided by observation of characteristic variations in line shape and linewidth as a function of controlled variations in P_b density, together with the observation of fine structure elements well distinct from ^{29}Si hyperfine structure.[9,10] Analysis of the results led to the conclusion that defects are distributed randomly, but small trends to clustering or self-avoiding behavior could not be excluded. While these studies suffered from limited P_b densities ($<10^{13}$ defects cm^{-2}), clearly, the newly revealed possibility[5] to enhance $[P_b]$ has opened new possibilities for the study of dipolar interactions. This is exploited in the present work, reporting on the first observation of angular dependent ($\vec{B}$ direction) properties in the P_b ESR signal as a result of dipolar interactions, thus establishing their relevance. A detailed analysis of the observed line width anisotropy is carried out by means of a statistical computational simulation model, based on the magnetostatic approximation of the local magnetic field. Comparison to the experiment has enabled us to infer information on the in-plane distribution of P_b centers and the interface strain relaxation correlated with P_b density.

II. EXPERIMENTAL DETAILS

Commercial 2-in. diam two-side polished (111) Si wafers (float zone; $>100\ \Omega$ cm; p-type; thickness$\sim$70 μm) were cut to sample slices of 2×9 mm^2, appropriate for ESR. After cleaning, the slices were oxidized in a high-vacuum laboratory facility[5] at $\sim$970 °C (1.1 atm 99.999% dry O_2; oxide thickness $\sim$42 nm). The oxidation was terminated by semiexponential cooling to room temperature in O_2 ambient (time constant $\sim$200 s). Subsequently, various ESR samples, consisting of $\sim$11 slices each, were submitted to a POA in H_2 (1.1 atm; 99.9999%) for $\sim$1 h—the P_b creation step[5]—at desired temperatures in the range 600–800 °C. The amount of additional created $P_b s$ can be ''tuned'' by appropriately choosing the temperature in this range. As all P_b defects are then automatically left passivated by H (ESR inactive) after such POA treatment, this was followed by exhaustive vacuum annealing ($<4\times10^{-7}$ Torr) at 620 °C for $\sim$1 h, which is known[11] to dissociate all existing P_bH entities without creating additional P_b entities. Conventional absorption-derivative K band ($\sim$20.5 GHz) ESR observations were made at 4.2 K as described elsewhere.[10] The P_b densities were determined by comparison of the signal intensity I, obtained by double numerical integration of the detected first derivative spectra dP_μ/dB (where P_μ is applied microwave power), to that of a comounted calibrated SiP standard signal, recorded in one trace. The accuracy on the obtained absolute P_b densities is estimated at $\sim$15%.

Five types of samples were studied. One sample, not submitted to H_2 POA, was used as an as-oxidized reference sample. The P_b density of this sample was measured as $(5.2\pm0.5)\times10^{12}$ cm$^{-2}\sim N_0$, as expected. Three other samples received the full treatment described above, using, however, different H_2 POA temperatures, T_{POA}, namely 690, 710, and 790 °C, resulting in P_b densities determined as (1.3 ± 0.1), (1.9 ± 0.2), and $(3.1\pm0.3)\times10^{13}$ cm^{-2}, respectively. At the latter density, the P_b creation by H_2 POA saturates, i.e., the P_b site density can not be increased by further increasing T_{POA}.[5] Finally, another sample received also a H_2 POA at 790 °C (highest P_b density) but the applied P_bH dissociation step was nonexhaustive (540 °C; 40 min) in order to leave the P_b bath partially passivated. The ESR-active density was determined as $(6.5\pm0.6)\times10^{12}$ cm^{-2}—close to N_0—representing approximately one fifth of the total P_b defect site density in the sample.

III. EXPERIMENTAL RESULTS

The behavior of the measured first derivative peak-to-peak linewidth ΔB_{pp} as a function of the angle φ_B between $\vec{B}$ and the interface normal $\vec{n}$ for the various samples is shown in Fig. 1. The angular behavior and line broadening mechanisms of the reference sample, i.e., as-oxidized state with $[P_b]\sim N_0$, was already studied extensively before.[12,13] This showed, among others, that superimposed on an angle-independent residual part of constant width, there is a distinct Gaussian component monotonously broadening with increasing φ_B, ascribed to a strain-induced Gaussian distribution in $g_\perp$ (see also next section). With increasing $[P_b]$, though, another trend is clearly revealed here: While the overall linewidth steadily increases, a significant dip in
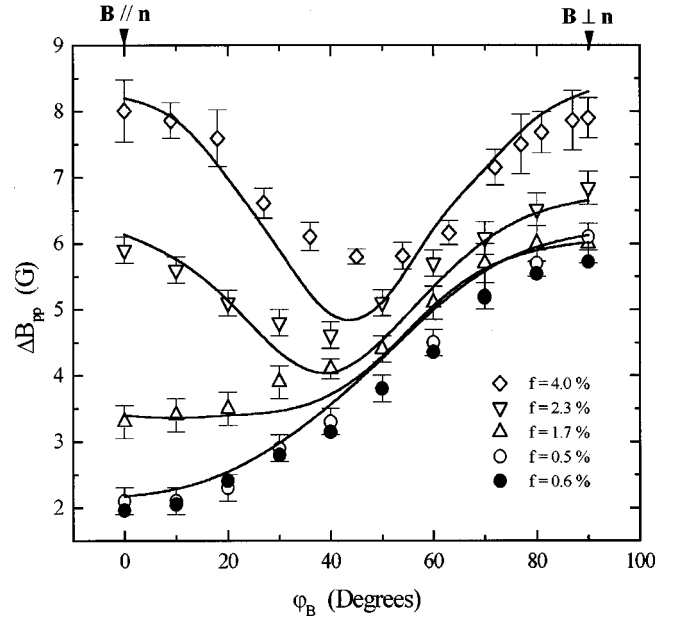

FIG. 1. Angular dependence of the P_b ESR peak-to-peak line-width for (111)Si/SiO$_2$ structures of different ESR-active P_b densities, determined as 0.52×10^{13} ($\bigcirc$), 1.3×10^{13} ($\triangle$), 1.9×10^{13} ($\triangledown$), 3.1×10^{13} ($\diamond$), 0.65×10^{13} ($\bullet$) cm^{-2}. Open symbols represent data obtained from fully depassivated samples. The filled symbols refer to a partially depassivated sample of which the total amount of P_b defect sites, regardless of their magnetic state, was determined as 3.1×10^{13} cm^{-2}. Solid lines represent the best fit to the open symbol data of a computer-calculated model based on the magnetostatic approximation of the local field, obtained by assuming a minimum interdefect separation larger than the third NN distance.

the linewidth-versus-φ_B pattern becomes prominent at φ_B $\sim$40°. The linewidth-versus-φ_B pattern of the partially depassivated sample is roughly the same as for the reference sample. Yet, for $\varphi_B\to90°$, a tendency to a smaller linewidth is observable.

The angular behavior of the line-shape factor κ $\equiv I/(A\,\Delta B_{pp}^2)$ is mapped for all samples in Fig. 2. Here, A is half the signal's peak-to-peak height. For large values of φ_B ($>$60°) the line-shape factor becomes nearly angular inde-
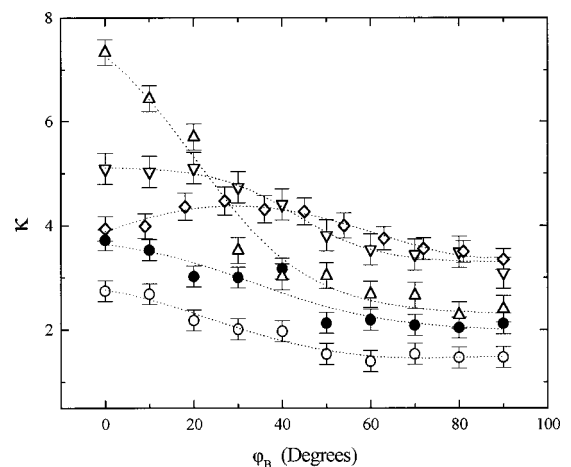

FIG. 2. Variation of the line-shape factor κ with magnet angle φ_B. Symbols have the same meaning as in Fig. 1. Dashed lines are guides to eye.
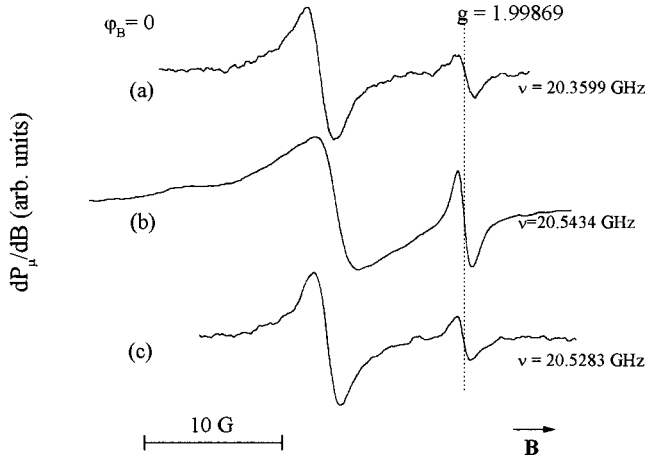
FIG. 3. Illustration of the influence of P_b density on the shape and width of the ESR signal for $\vec{B}\perp(111)$Si/SiO$_2$ interface. (a) as-grown reference oxide interface with $[P_b]=0.52\times10^{13}$ cm^{-2}; (b) $[P_b]\sim1.3\times10^{13}$ cm^{-2}, obtained by H$_2$ POA at 960 °C followed by exhaustive depassivation in vacuum (620 °C, ~1 h;) (c) sample *saturated* with P_b defects (3.1×10^{13} cm^{-2}) realized by H$_2$ POA at 790 °C (exhaustive creation), followed by only partial depassivation (540 °C, 40 min), resulting in an ESR active density of ~6.5 $\times10^{12}$ cm^{-2}.

pendent while monotonically increasing with P_b density. The measured κ values in this region span the range from the Gaussian line shape factor ($\kappa^G=1.03$) observed for the lower P_b densities, to the Lorentzian value ($\kappa^L=3.63$) pertaining to the higher densities. For small φ_B values, however, κ displays unusually large variations with $[P_b]$. Starting from well below κ^L a maximum value of $\kappa=7.3$ is reached for $[P_b]=1.3\times10^{13}$ cm^{-2}. With further increasing P_b density, κ decreases and apparently tends to κ^L. The line-shape factor of the partially depassivated sample appears to have undergone a significant constant shift upward as compared to the reference sample. Clearly, as indicated by the κ data, there is a drastic change in line shape with growing H$_2$ POA budget, i.e., advancing creation of P_b defects. This is illustrated in Fig. 3, showing two spectra observed with $\varphi_B=0$ on the reference sample (a) and the sample of $[P_b]\sim1.3 \times10^{13}$ cm^{-2}, submitted to H$_2$ POA at 690 °C. Curve (c) exposes the effect of partial passivation, i.e., reduction in ESR-active P_bs.

Generally, g values are determined using the resonance condition $h\nu=g\beta B$, where h is Plank's constant, ν the microwave frequency, β the Bohr magneton, and B the resonance field read at the zero crossing of first derivative absorption spectrum. Henceforth, we will refer to this quantity as the *zero crossing g value*, g_{zc}. Previously, the P_b g tensor was found to exhibit axial (C_{3v}) symmetry.[2] The g map for rotation of $\vec{B}$ from $\vec{B}\|\vec{n}$ ($\varphi_B=0$) towards any direction perpendicular to $\vec{n}$ ($\varphi_B=90°$) contains one single branch, obeying

$$g=\sqrt{(g_\|\cos\varphi_B)^2+(g_\perp\sin\varphi_B)^2},\qquad(1)$$

with principal values inferred as $g_\|=2.00136\pm0.00003$ and $g_\perp=2.0088\pm0.0001$.[14] In the present work, Eq. (1) was fitted to the observed of g_{zc}-versus-φ_B data, with $g_\|$ and $g_\perp$ as free adjustable parameters. The obtained values of $g_\|$ and $g_\perp$
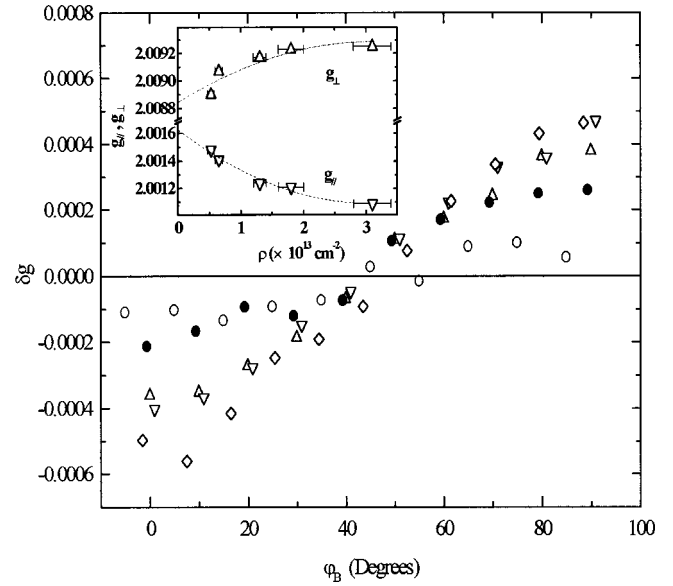

FIG. 4. Angular dependence of the shift δg [cf. Eq. (2)] of the P_b ESR signal for various P_b densities. The meaning of the symbols is the same as in Fig. 1. The inset shows the variation of the g value with increasing density for the $g_\|$ and $g_\perp$ values inferred from fitting the g_{zc}-vs-φ_B data using Eq. (1). The dotted lines represent least-squares polynomial fits based on Eqs. (6) and (8).

appear to vary systematically with the P_b density as shown in Fig. 4 (inset), where extrapolation toward $[P_b]=0$ (see next section), yields $g_\|^0=2.0016\pm0.0001$ and $g_\perp^0=2.0088 \pm0.0001$. The variations in g_{zc} may be specified with respect to these values in terms of the shift

$$\delta g=g_{zc}-\sqrt{(g_\|^0\cos\varphi_B)^2+(g_\perp^0\sin\varphi_B)^2}.\qquad(2)$$

The variation of δg with φ_B and P_b density is shown in Fig. 4. Positive shifts are observed towards the $g_\perp$ direction while for $\varphi_B\to0$ ($g_\|$ direction) negative shifts are observed. For all densities, δg crosses zero at $\varphi_B\sim45°$. The magnitude of the shift increases monotonically with P_b density in both the $g_\|$ and $g_\perp$ direction.

The magnetic susceptibility χ of the P_b spin system was determined for all fully depassivated samples with enhanced P_b density by measuring I as a function of temperature T in the range 1.6-30 K. Generally, Curie-Weiss type behavior is expected, i.e., $I\sim\chi\sim(T-T_c)^{-1}$, with T_c the Curie temperature. The measured values are shown in Fig. 5. The susceptibility appears to differ only very slightly from a pure Curie-type behavior, showing a very slight tendency for a positive $T_c(<1.3\pm0.8$ K), i.e., ferromagnetic coupling. Within experimental error, neither angular dependence in T_c nor any pronounced trend with varying $[P_b]$ could be discerned. These susceptibility measurements assure that no significant spontaneous magnetic ordering occurs within the P_b system at low T.

Previous works have shown that the standard as-grown interface is remarkably flat: it consists of single crystallographic planes with typical dimension of a few hundred Å across, terminated by ledges of one to three atomic steps high.[15] We have performed room-temperature atomic force microscopy measurements on the H$_2$ POA treated samples after etch off of the oxide layer. No deviation could be de-
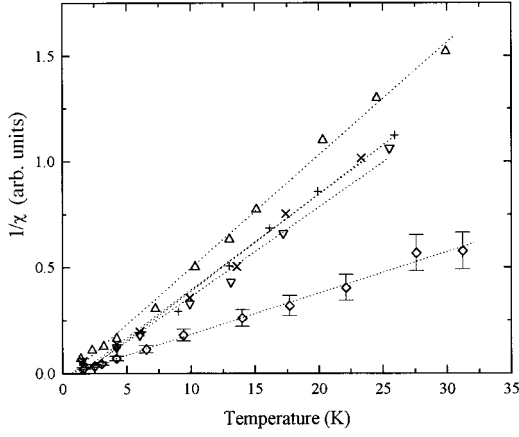
FIG. 5. The magnetic susceptibility of the P_b spin system for various defect densities. The usage of symbols is the same as in Fig. 1. Open symbols refer to measurements for $\varphi_B = 40°$; vertical and diagonal crosses represent measurements on the sample of $[P_b]$ $= 1.9 \times 10^{13}$ (∇) for $\varphi_B = 0°$ and $\varphi_B = 90°$, respectively. Dotted lines represent least squares linear fits.

tected, e.g., in terms of increased roughness, asperities, ledges, of the exposed planar Si surface within 0.2–0.3 nm as compared to that of the as-grown $(111)Si/SiO_2$. Moreover, the ESR spectra reveal no trace of P_b defects oriented in any of the other possible equivalent (111) directions (unpaired sp^3 hybrid at ~19° with the interface plane).[16] Hence, we conclude that all samples H_2 POA-treated exhibit the same abrupt planar interface structure as occurring in the as-grown state.

IV. ANALYSIS AND INTERPRETATION

A. P_b linewidth

From φ_B dependence observations, a previous study had concluded that the P_b ESR line width at the standard $(111)Si/SiO_2$ interface consists of mainly two superposed contributions.[12,13] Next to an angle independent residual part, approximately Lorentzian shaped, a considerable amount of Gaussian type broadening monotonically growing for $\vec{B}$ tilting towards the $g_\perp$ direction was identified. Our reference sample exhibits the same behavior (cf. Fig. 1). The Gaussian part is attributed to strain induced variations in the g tensor, predominantly in $g_\perp$. Insight was provided by the work of Watkins and Corbett.[17] From molecular orbital calculations, they showed that strain induced variations in the microscopic geometry of a dangling-bond type defect—like P_b—results in a perturbation on $g_\perp$, but, to first order, not on $g_\parallel$. The supposedly Lorentzian residual linewidth contribution was mainly attributed to unresolved ^{29}Si superhyperfine broadening. Later, more in-depth line-shape studies of the residual line for $\vec{B} \perp (111)Si/SiO_2$ interface[9,10] revealed clearly the influence of a relative small P_b density-dependent dipolar broadening contribution in the residual line. In this study, among others, it was pointed out that the residual line, stripped of dipolar broadening, is best approximated by a Voigt like profile of $\Delta B_{pp}^R = 1.29$ G, the Lorentzian and Gaussian broadening respectively being given by $\Delta B_{pp}^{R,L}$ $= 0.67$ G and $\Delta B_{pp}^{R,G} = 0.90$ G. Importantly, another study[1]

on the as-oxidized P_b ESR line shape demonstrated the presence of some strain-induced spread on the $g_\parallel$ value as well.

B. Dipolar broadening: Computational approach

A key point of the present paper is the observed φ_B dependence of the P_b ESR parameters, emerging with increasing P_b density. It is our aim to show that this is due to the growing impact of the intradipolar interaction within the P_b system. As to our knowledge, no exact analytic quantum mechanical calculation for the angular dependence of the dipolarly broadened ESR line shape for a diluted 2D spin system exists,[8,10,18] the obtained results for ΔB_{pp} as function of φ_B are analyzed using a computer calculated statistical model, based on the magnetostatic approximation of the local magnetic field.[19,20] In this approximation, we consider a number of dipoles $\vec{\mu}_k$ distributed over a 2D plane of lattice sites. The dipolar broadening then is ascribed to variations in local magnetic field acting upon the individual dipoles due to variations in spatial distribution and orientation of the surrounding dipoles over the interface. Accordingly, when dipolar broadening dominates, the resonance line shape will reflect the shape of the local field distribution. For practical calculations, the local magnetic field B_{dip} sensed by a dipole $\vec{\mu}_k$, due to the vicinity of surrounding dipoles $\vec{\mu}_j$, is approximated by the sum of their independent static contributions B_{jk}, parallel to the applied field $\vec{B}$, i.e., $B_{dip} = \Sigma_j B_{jk}$.

Starting from the classical expression for the interaction energy between two magnetic dipoles and using the quantum mechanical equivalent for the electronic dipole moment of an electron of spin $\vec{S}$, $\vec{\mu}_k = g\beta\vec{S}$, one can show that

$$B_{jk} = \pm \frac{3}{2} \frac{g\beta}{2\pi r_{jk}^3} (1 - 3\cos^2\theta_{jk}). \quad (3)$$

Here, an extra factor $\frac{3}{2}$ is inserted to account for the dynamical character of the local field,[21] a quantum mechanical result. μ_0 represents the vacuum permeability and θ_{jk} is the angle between $\vec{B}$ and the vector $\vec{r}_{jk}$ interconnecting the two magnetic moments. The sign of B_{jk} is determined by the component S_z of $\vec{S}$ along $\vec{B}$. Together with other line broadening mechanisms, the spread in local field—the local field histogram—will determine the line width and shape of the observed resonance line.

The configured model is implemented in a computational program used to approximate the local field histograms for the P_b defects occurring at the 2D $(111)Si/SiO_2$ interface. For that end, a circular region of fixed area size is considered around a central P_b defect located in an unreconstructed {111} Si plane enclosing N Si atom sites. N needs to be taken sufficiently large to ensure results independent of the size of the sample region, i.e., typically several hundred up to a few thousand. The Si sites form a triangular net of lattice parameter $a_L = 3.846$ Å, over which the P_b defects are in principal (*vide infra*) considered randomly distributed. (So, no subsets of surface Si sites as allowed P_b hosts are considered.[10]) It is obvious from a comparison between the surface density of Si lattice sites in the {111} Si plane N_a ($= 7.830 \times 10^{14}$ cm^{-2}) and the occurring areal P_b densities that only a fraction of these sites is the host of P_b defects. We may write the average number of defects in a circular

region of fixed area as $\bar{n} = f\mathrm{N}$, where $f \equiv [P_b]/\mathrm{N}_a$ is the fractional occupancy which in turn will be fixed by the desired P_b density. As the distribution of defects over the net is, in principle, random, the number n of P_b defects within equally sized circular regions of the interface may fluctuate around $\bar{n}$. Hence to simulate reality we will have to average over numerous such circular regions, statistically differing in the number of P_b defects enclosed and their distribution over the region. To account for these fluctuations, the starting point in the procedure of generation of a P_b configuration (P_b assignment) over a circular region will be the individual site occupancy probability p. Additionally, it is enabled to impose restrictions on the allowed interdipole distance. This is done by defining a nearest neighbors (NN) exclusion range n_{ex}, excluding any pair of defects in the net to be within or at the n_{ex}th NN distance.

To obtain a dipolar histogram, the dipolar local field contribution of a representative random sample from the collection of all possible configuration is taken into account. The calculation procedure for a given desired f and NN exclusion range n_{ex} then consists of the following parts. First, p is determined such that random placement of defects over the virtual {111} Si plane region respecting the imposed n_{ex} restriction results in a lattice occupation equal to the desired net fractional occupation f. For $n_{\mathrm{ex}}=0$, the defects are perfectly randomly distributed and p is just equal to the desired f. However if $n_{\mathrm{ex}}>0$, spatial correlations between the defects are introduced and since all lattice sites are no longer accessible, p needs to be chosen somewhat larger than f. This is easily attained by trial and error within 1% accuracy. In a second step, the local field contributions for a large number of P_b arrangements ($\sim 10^5$) are calculated using Eq. (3). Finally, the obtained local field contributions are organized into a histogram of resolution 0.007 G and field width 70.000 G. By virtue of thorough accumulation and the high resolution these discrete histograms show a continuous absorption-like line-shape contour. We will refer to the width at half height of these *bare* dipolar histograms and their derivative peak-to-peak width as ΔB^{dip} and $\Delta B_{pp}^{\mathrm{dip}}$, respectively.

Each individual P_b arrangement is obtained by scanning through the net of N lattice sites in a fixed sequence. During this sequence a defect can be *randomly* assigned to each Si lattice site in accordance with the nominal occupation probability p. For each assigned defect, its spin state is again assigned randomly. Since no significant ordering of the magnetic spin state is present (cf. Fig. 5), the Boltzmann factor is used to determine the spin state. Because of the small variations in the experimental conditions, the Boltzmann factor is approximated as a constant $n_-/n_+ = e^{g\beta B/kT} = 1.26$. Here, n_- and n_+ represent the probability of finding a certain defect in the $S_z = -\frac{1}{2}$ and $\frac{1}{2}$ state, respectively, $g\beta B$ is the Zeeman-splitting energy (for $B \sim 7300\,\mathrm{G}$), and k Boltzmann's constant. When an exclusion range n_{ex} is defined, the nominal probability p of all enclosed NN Si sites within n_{ex} distance is set to zero as soon as a defect is assigned, thus excluding any pair of defects in an array to be within the n_{ex}th NN distance. This routine allows for a random fluctuation in n. For $n_{\mathrm{ex}}=0$, these fluctuations are described by the binomial distribution $P(n,N,p) = \binom{n}{N} p^n (1-p)^{N-n}$, where, the factor $\binom{n}{N} = N!/(N-n)!n!$ represents the number of pos-

sible arrangements containing n defects distributed over N Si sites. For a fixed value of N, p is chosen such that $P(n,N,p)$ reaches its maximum value at $\bar{n}$. However, a restriction of $n_{\mathrm{ex}}>0$ introduces spatial correlation and therefore the above mentioned statistic probabilities will be more or less distorted depending on the value of n_{ex}. The introduction of an exclusion range causes the defects to be more regularly distributed over the interface, resulting in a smaller spread in n than prescribed by the binomial distribution.

For all P_b densities considered, the angular dependence of ΔB^{dip} of the calculated local field histograms is found to exhibit a typical dip at $\varphi_B \sim 40° - 45°$ indicative of the qualitative validity of the applied model: Such anisotropy with respect to $\vec{B}$ is a well-known expected[6,7,22] characteristic of dipolar interaction within a 2D system of like magnetic spins (similar for electrons and nuclei), reflecting the *lattice-averaged* effect of the basic anisotropy—the ''magic angle'' $[\theta_{ij} = \cos^{-1}(1/\sqrt{3}) = 54.7°]$ epic—in the classical dipole interaction [cf. Eq. (3)] between two magnetic moments. As a quantitative test, the predictions of our model were compared to the quantitative results of two previous calculations. First, comparison was made with the theoretical work of Kittel and Abrahams[23] on dipolar broadening for a diluted, randomly populated 3D cubic lattice, based on the successful method of moments as developed by Van Vleck.[7] For $f \ll 1$, the calculated moments of dipolar broadening for $\vec{B} \| (100)$ were shown to be compatible with a cutoff Lorentzian line of half width at half maximum height $\frac{1}{2}\Delta B^{\mathrm{dip}} = 5.3fA$, with $A = g\beta/a^3$. In this case, f represents the 3D fractional occupancy and a is the cubic lattice parameter. We have compared the theoretically predicted values for ΔB^{dip} with the simulated ones for the range $0 < f \leq 0.01$. For that purpose, our computational scheme was extended to the case of a 3D cubic lattice. While both the computational and theoretical model predict that the width ΔB^{dip} varies linear with f, the computational values are larger by a constant factor of 1.6 ± 0.3. Second, the present computational model predictions for the local field histogram, as based on static approximation of the local field, were compared to those of another 2D computational model, based on the exact solution of the Hamiltonian.[10] The main aim of the latter study, also performed for the P_b defect at the (111)Si/SiO$_2$ interface, was the evaluation of dipolar broadening and line shape variations as a function of the P_b density for $\varphi_B = 0$. Limited computational power, however, restricted these calculations to $f < 0.004$. For the small dipolar contributions $\Delta B_{pp}^{\mathrm{dip}}$ in this range, it appears that the total width ΔB_{pp} can be approximated by $\Delta B_{pp} \cong \Delta B_{pp}^{\mathrm{dip}} + \Delta B_{pp}^R$. Again, the $\Delta B_{pp}^{\mathrm{dip}}$ values obtained by static local field approximation, were found larger than the values estimated from the previous computational model[10] by a factor of 1.6 ± 0.5.

The obvious conclusion from these two comparisons is that the dipolar contribution as predicted by our static local field approximations overestimates the dipolar broadening by a constant factor, which, reassuringly comes out the same for both comparisons. This deviation is accounted for by a correction factor K determined from optimized fitting of the line width data (*vide infra*) as $K = 1.7 \pm 0.2$. The required correction factor is seen as originating from the particular underly-
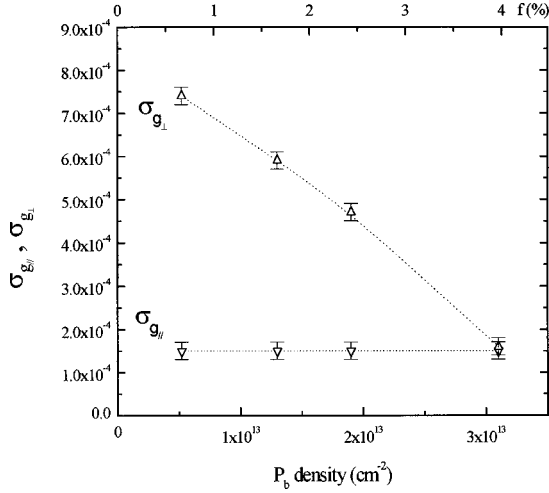
FIG. 6. Obtained values for the strain-induced spreads $\sigma_{g\parallel}$ (∇) and $\sigma_{g\perp}$ ($\triangle$) on $g_\parallel$ and $g_\perp$, inferred from fitting the data in Fig. 1 using a computer-calculated model based on the magnetostatic approximation of the local field. Gaussian distributions were assumed. Dotted curves guide the eye.

ing assumption, i.e., static approximation of the local field which neglects spin-correlation effects.

Along the outlined scheme, dipolar histograms were calculated to simulate the observed line width dependence. The considered circular {111}Si regions typically contained 2515 lattice sites (radius $r = 10$ nm). For each P_b density, histograms of the local dipolar field distribution were composed by evaluating numerous ($\sim 10^5$) P_b arrays for a fixed nominal occupation probability p and NN exclusion range n_{ex}. For a fixed value of n_{ex}, p was chosen such that $\bar{n}/N$ was equal to the desired f within 1%. The latter is allowed to vary from the experimentally observed one within the estimated experimental error on P_b density.

C. Dipolarly broadened P_b line shape

The calculated histograms are used to simulate the observed dipolar spectra. This requires convolution with a characteristic line incorporating the known various other line broadening mechanisms, i.e., residual and strain-induced line broadening effects. Two approximations are made: First, it is assumed that the strain component $\Delta B_{pp}^{\mathrm{SB}}$ of the linewidth is purely Gaussian and can be related to distributions in $g\parallel$ and $g_\perp$. To a first approximation, the angular dependence of $\Delta B_{pp}^{\mathrm{SB}}$ can be expressed as a function of $\sigma_{g\parallel}$ and $\sigma_{g\perp}$ by[12]

$$\Delta B_{pp}^{\mathrm{SB}} = \frac{2h\nu g_\parallel \cos^2(\varphi_B)}{\beta g^3}\sigma_{g\parallel} + \frac{2h\nu g_\perp \sin^2(\varphi_B)}{\beta g^3}\sigma_{g\perp}, \quad (4)$$

where $\sigma_{g\parallel}$ and $\sigma_{g\perp}$ represent the standard deviation on the supposedly Gaussian distribution in $g_\parallel$ and $g_\perp$, respectively. This approximation is a generalized approach of the one presented in Ref. 12, where $\sigma_{g\parallel} = 0$ was assumed. Second, the Voigt-like approximation of the residual line is assumed to be void of strain broadening contributions as is done in Ref. 1. The effect of strain broadening is incorporated by adding it to the Gaussian contribution of the residual line $\Delta B_{pp}^{R,G}$ along the Gaussian addition rule $(\Delta B_{pp}^{R,G})^2 + (\Delta B_{pp}^{\mathrm{SB}})^2$.

The various parameters involved were optimized to fit the measured φ_B dependence of ΔB_{pp} (Fig. 1). For investigated n_{ex} values ranging from 0 to 6, a global satisfactory fitting is only achieved with $n_{\mathrm{ex}} = 3$, which results are shown in Fig. 1 (solid lines). The obtained fitting results for the strain-induced spread on $g_\parallel$ and $g_\perp$ are shown in Fig. 6 as function of the P_b density. The inferred values of $\sigma_{g\parallel}$ and $\sigma_{g\perp}$ for $[P_b] \sim N_0$ (reference sample) are found to be in good agreement with the previously reported values.[1,12] The emerging constant value $\sigma_{g\parallel} = 0.00015 \pm 0.00002$ is to be compared to the reported value of $\sigma_{g\parallel} = 0.00032$.[1] Here, it needs to be remarked that the latter value was attained in an attempt to simulate the apparent asymmetry of the P_b signal. A half Gaussian distribution of width 0.00032 on $g_\parallel$ was proposed as an approximation of a skewed Gaussian distribution. In the present study, however, the effect of asymmetry is neglected and, by applying a *full* Gaussian distribution, it is necessary to take into account an extra factor of about two when comparing. The deduced $\sigma_{g\perp}$ value 0.00074 ± 0.00002 for the reference sample is also in good agreement with the previously reported value of $\sigma_{g\perp} = 0.00075 \pm 0.00010$.[12] However, a remarkable finding is that to fit the data consistently, $\sigma_{g\perp}$ needs to be gradually decreased with increasing P_b density. The decrease is approximately linear with the P_b density, to result, for the highest density sample ($[P_b] \sim 3.1 \times 10^{13}$ cm^{-2}), in $\sigma_{g\perp} = \sigma_{g\parallel}$.

D. Resonance position

As well as for the line width, the simulations predict a dipolar angular dependence of the resonance zero crossing value g_{zc} superposed on the known g tensor anisotropy. Relative to the unperturbed values, perturbations can cause an apparent shift δB in the observed resonance field value (zero crossing) that can be expressed equivalently as a shift δg in g value using

$$g + \delta g = \frac{h\nu}{\beta(B - \delta B)}. \quad (5)$$

Neglecting the effect of exchange narrowing, the origin of dipolarly induced resonance shifts is simply the mean dipolar field $\langle B_{\mathrm{dip}}\rangle$,[22] producing a shift $\delta B = -\langle B_{\mathrm{dip}}\rangle$ in resonance field. In order to quantify the observed shifts, it is important to define a reference. This is obtained by extrapolation to the resonance position void of any dipolar shift, i.e., $[P_b] \rightarrow 0$. As representative reference values, the extrapolated $g_\parallel$ and $g_\perp$ from the zero crossing g-map fittings are used (cf. inset in Fig. 4). In analogy with Eq. (5), these g values should obey the equations

$$g_{\parallel,\perp}^0 + \delta g_{\parallel,\perp}^{\mathrm{dip}} = \frac{h\nu}{\beta} \frac{1}{\dfrac{h\nu}{\beta g_{\parallel,\perp}^0} + \langle B_{\mathrm{dip}}\rangle_{\parallel,\perp}}. \quad (6)$$

Here $g_{\parallel,\perp}^0$ represent the dipolarly unperturbed (reference) values of $g_\parallel$ and $g_\perp$ and $\delta g_{\parallel,\perp}^{\mathrm{dip}}$ the dipolarly induced shifts on these values for the $\varphi_B = 0°$ and $\varphi_B = 90°$ directions. The contribution $\delta g_{\parallel,\perp}^{\mathrm{dip}}$ is P_b density dependent, with $\delta g_{\parallel,\perp}^{\mathrm{dip}} \rightarrow 0$ for $[P_b] \rightarrow 0$. So, the left-hand side of Eq. (6) simply repre-
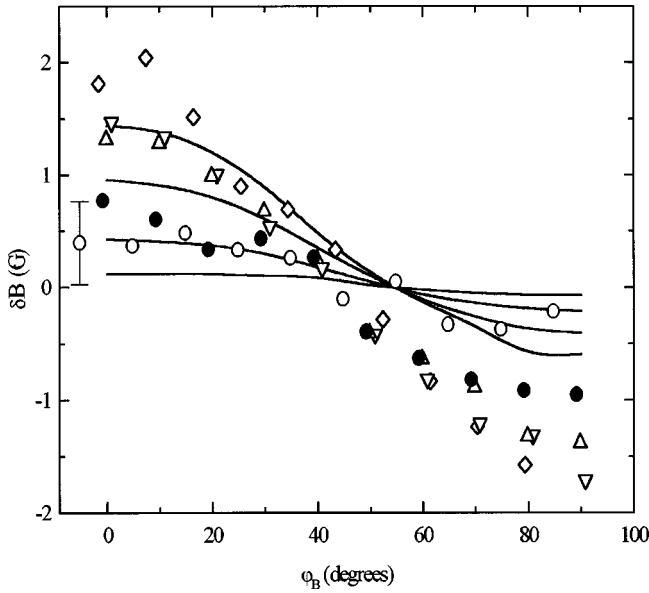
FIG. 7. Angular dependence of the shift in resonance field at zero crossing of the P_b ESR signal, [see Eq. (9)]. The meaning of the applied symbols is the same as in Fig. 1. Solid lines represent the values obtained from the mean dipolar fields as inferred from fitting the data in Fig. 1 using a computer-calculated model based on the magnetostatic approximation of the local field.

sents the observed P_b density dependence of $g_\parallel$ and $g_\perp$. For a 2D paramagnetic system of $f=1$, one can show that[20]

$$\langle B_{\text{dip}} \rangle_\parallel = -|\vec{\mu}_\parallel| \sum_n \frac{1}{r_n^3}$$

$$\langle B_{\text{dip}} \rangle_\perp = -\frac{|\vec{\mu}_\perp|}{2} \sum_n \frac{1}{r_n^3}. \quad (7)$$

Here, $\vec{\mu}_\parallel$ and $\vec{\mu}_\perp$ are defined by $\vec{M}_\parallel = N_s \vec{\mu}_\parallel$ and $\vec{M}_\perp = N_s \vec{\mu}_\perp$, where $\vec{M}_\parallel$ and $\vec{M}_\perp$ represent the magnetization in the $\varphi_B = 0°$ and $90°$ direction, respectively, and N_s the density of paramagnetic species. $\Sigma_n 1/r_n^3$ is called the lattice sum. The summation is taken over all paramagnetic species encircling a fixed central site with r_n the distance relative to that central site. For $f=1$ summing over all species is equivalent to summing over all lattice sites. For the present case of P_b defects, i.e., $f<1$, we still do admit there to exist a proportionality of $\langle B_{\text{dip}} \rangle$ with the lattice sum. From numerical evaluation of the lattice sum, the relationship between the lattice sum and paramagnetic species appears to be closely quadratic. Hence, to a first approximation, we propose

$$\langle B_{\text{dip}} \rangle_{\parallel, \perp} = A_1 \rho + A_2 \rho^2, \quad (8)$$

where A_1 and A_2 are adjustable parameters and ρ is the areal defect density. This expression is employed in fitting the right-hand side of Eq. (6) to the observed $g_\parallel$ and $g_\perp$ P_b density dependence (dotted line in the inset of Fig. 4). The A_1 and A_2 values come out equal for the $\varphi_B = 0°$ and $90°$ directions within the regression accuracy, taken as confirmation of the unique relationship between $[P_b]$ and $\langle B_{\text{dip}} \rangle_\parallel, \langle B_{\text{dip}} \rangle_\perp$. The respective values for A_1 and A_2 are $(-1.3 \pm 0.5) \times 10^{-13}\,\text{G cm}^2$ and $(0.21 \pm 0.14) \times 10^{-26}\,\text{G cm}^4$

for $\varphi_B = 0°$, and $(1.0 \pm 0.5) \times 10^{-13}\,\text{G cm}^2$ and $(-0.17 \pm 0.14) \times 10^{-26}\,\text{G cm}^4$ for $\varphi_B = 90°$. The inferred values for $g_\parallel^0$ and $g_\perp^0$ are 2.0016 ± 0.0001 and 2.0088 ± 0.0001, respectively. These g values represent the dipolarly unperturbed resonance positions, i.e., the true principal values of the intrinsic g tensor. Shifts in resonance field position are defined with respect to these values by the expression

$$\delta B = B_{zc} - \frac{h\nu}{\beta \sqrt{(g_\parallel^0 \cos \varphi_B)^2 + (g_\perp^0 \sin \varphi_B)^2}}. \quad (9)$$

This results in Fig. 7, showing the experimentally observed shift in field position. The solid lines represent the deviations in zero crossing field position as predicted by the simulation. Though not perfect quantitatively, the qualitative agreement is obvious and quite reasonable in view of the experimental error. Towards the $\varphi_B = 90°$ direction, though, there is larger deviation in magnitude. This may have several origins. One reason could be errors in the extrapolated $g_\perp^0$ and $g_\parallel^0$ values, which could artificially induce such systematic deviations. In addition, it should be remarked that the reading of the variation in g competes with experimental accuracy. In another view, the deviations may also have resulted from effective shifts in the zero crossing g due to asymmetry in the g distribution, as reported previously.[1] Finally, a slight deviation from pure Curie-type behavior might also induce some disagreement.

V. DISCUSSION

It is generally accepted that the driving agent for the occurrence of P_b defects at the interface of standard (111)Si/SiO$_2$ is the existence of intrinsic interfacial stress.[1] In this perspective, among others, the inherent P_b density (N_0) pertinently reflects the invariable natural mismatch between the c-Si and the standardly grown a-SiO$_2$ layer due to the difference in molar volume.[1] Although the reaction mechanism is unknown, the eventual effect of the additionally applied H$_2$ POA anneal is an irreversible interfacial bond rupture, yielding additional defects indistinguishable from the pre-existing P_b defects.[5] As discussed below, two major results presently attained, i.e., the self-avoiding defect behavior and the gradual decrease of the strain broadening in the $g_\perp$ direction with increasing $[P_b]$, may find a consistent interpretation within this understanding of the defect-strain relationship. Moreover, this interpretation provides a comprehensive insight into the H$_2$ POA creation mechanism of P_bs.

The inference that the P_b defects are distributed in a self-avoiding manner strongly indicates that the P_b creation mechanism is spatially selective. As suggested earlier,[5] a possible interpretation might start from the existence of particularly vulnerable, i.e., strained, bonds at the interface. Then, if one of the effects of hydrogen during POA would be the rupture of such bonds at the Si/SiO$_2$ interface, it would allow the system to locally release the stress associated energy, thus locally relaxing the interface. The observed irreversible nature of the H$_2$ POA creation mechanism might well reflect the irreversibility associated with such relaxation process. At a particular broken bond site (e.g., a P_b defect created), the attendant relaxation is expected to range spa-

tially beyond the single atom hosting the broken bond. The extent of the relaxing influence in its turn will beneficially influence the stability of the surrounding bonds, which could lead to a type of self-avoiding defect behavior. As the density of P_b defects gradually increases, the locally relaxed defect surroundings start to percolate the interface, hence gradually relaxing the global interface structure. As suggested previously,[5] this might offer a possible explanation of the saturation behavior of the H_2 POA creation mechanism. The ultimate P_b density, in this view, is set by the amount of defects necessary to sufficiently percolate, i.e., relax, the interface, leaving all left saturated bonds sufficiently invulnerable for H_2 attack. In this view, the observed attendant decrease of the strain broadening contribution, as reflected in $g_\perp$, may appear natural. It would strongly indicate a gradual decrease of average interface stress with increasing P_b density. As observed, though, $\sigma_{g\parallel}$ appears not to be affected by such interface relaxation process. As outlined, this result can be straightforwardly attributed to the inherently smaller sensitivity of $g_\parallel$ to strain or, in a different point of view, might indicate the residual spread on $g_\parallel$ to be of a different nature.

It is noteworthy that precisely at the P_b density saturation value, $\sigma_{g\perp}$ reaches its minimum value equal to $\sigma_{g\parallel}$. This suggests that the maximum attainable relaxation by the applied H_2 POA is reached. According to the fitting results described in Sec. IV C, the estimated extent of the relaxing influence by the creation of a single P_b defect would be about the 3rd NN distance, i.e., $2a_L$. This value is in excellent agreement with previously reported observations of dipolar fine structure doublets assigned to the interaction of fourth and fifth NN defect pairs- no first, second, and third NN pairs could be discerned.[10] For a P_b density of 3.1 $\times 10^{13}$ cm^{-2} ($f = 0.04$) and with $n_{ex} = 3$ imposed, defects distributed randomly over a {111}Si plane efficiently cover the whole interface area. From the simulations, it was found that in this case, 64% of all lattice sites are within third NN distance to occurring P_b defects, while 83% and 88% of all lattice sites are within fourth NN and fifth NN distance, respectively, of a defect. Perhaps, it is important here to mention that the exclusion range value was obtained from the assumption that, to a first approximation, the self-avoiding character is treated ''hard-sphere''-like, independent of the local defect surrounding. Hence, the reported value $n_{ex} = 3$ should perhaps be considered as indicative rather than absolute.

A next interesting aspect is the comparison of the partially passivated sample with the standard reference sample. Both samples contain approximately the same density of (dipolarly interacting) ESR active P_b defects. In view of the above interpretation, the interface relaxation is expected to be related to the total amount of broken bonds, regardless of their spin state, i.e., passivated by hydrogen or not. Along this view, the P_b system in the reference sample would reside at a more strained interface than the one in the *partially* depassivated sample. We will refer to the latter sample as more *relaxed*. Keeping in mind the drastic decrease in $\sigma_{g\perp}$ with the increasing density of unpassivated P_b's, as exposed in Fig. 6, it is interesting to compare the amount of strain broadening in the $\varphi_B = 90°$ direction for both of samples. The observed line width versus φ_B patterns depicted in Fig. 1

show only a slight difference in the $g_\perp$ direction. For $\varphi_B \rightarrow 90$, there is a slight decrease in ΔB_{pp} of the relaxed sample relative to the reference specimen. Based on their almost equal density of unpassivated P_b defects we may assume equal dipolar broadening; hence, the decrease of line width is to be attributed solely to a decrease in strain broadening. The change in relative contribution of these two broadening mechanisms is affirmed by the attendant change in line shape (cf. Fig. 2). From the observed decrease in line width, estimated at ~0.5 G in the $g_\perp$ direction, one calculates a decrease in $\sigma_{g\perp}$ from 0.00074 for the reference sample to 0.00067 for the relaxed sample. Remarkably, this reduction comes out significantly smaller than the observed decrease in $\sigma_{g\perp}$ as function of the P_b density for the fully depassivated samples, as shown in Fig. 6. The latter behavior would prescribe $\sigma_{g\perp}$ to decrease to ~0.00015. Obviously then, the presence of hydrogen in the Si/SiO$_2$ structure, among others, passivating about 80% of the P_b defects at the interface, influences the $P_b g$ value distribution as well.

Various interpretations can be given. In a first one, one might suggest that the g distribution pertaining to the subset of depassivated P_b defects is not representative for the whole P_b system. A hint comes from experimental observation of the existence of spread in the activation energy for the hydrogen passivation and depassivation of P_b defects reported previously.[24] The very existence of this spread is attributed to change in local defect geometry, i.e., strain, affecting the bond strength via weak orbital rearrangements. In the case of the relaxed sample, being submitted to partial non-exhaustive dissociation, only a certain sub ensemble (lowest activation energy tail) will be selected out. With the known coupling between the defects atomic morphology, activation energy and actual g value, the selected subensemble might also not be representative for the whole P_b bath in terms of g spread. As an ''extremized'' subset, their $\sigma_{g\perp}$ spread might well exceed that of the total P_b bath. Second, one may presume that the global interface relaxation is dependent upon the amount of hydrogen at the interface and, possibly, in the oxide. Hence, relaxation could be affected by the extend and degree of completion of passivation/depassivation treatments. However, in the light of the observed strict irreversibility of P_b creation under POA in H_2, the latter suggestion is considered less likely.

VI. CONCLUSIONS

The application of appropriate POA treatments in H_2 of standard thermal (111)Si/SiO$_2$ leads to enhanced P_b densities without significant degradation of the planar interface geometry. These enhanced P_b densities enabled observation of distinct P_b density-dependent anisotropy in the ESR spectra with respect to $\vec{B}$, providing direct experimental evidence for dipolar interactions within the 2D magnetic P_b system. A field angle dependence of the ESR spectra is observed in linewidth, line shape and g shifts. Measurement of the magnetic susceptibility for various P_b densities bear out that the exchange interaction is negligible and no significant magnetic ordering is present, even at low temperatures. A slight tendency to ferromagnetic coupling ($T_c < 1.3 \pm 0.8$ K), however, cannot be excluded.

Within the framework of a computational model, the ob-

served dependencies of the linewidth and g shift were successfully simulated. The core of these simulations is a statistical approximation of the dipolarly induced local field distribution. These simulations indicate that defects are distributed in a self-avoiding manner. Optimal fitting of all experimental results is only achieved by applying an interdefect exclusion range of third NN distance for all defects. The fitting procedure is complicated by the existence of the angular dependent line broadening arising from strain-induced spread in g. An overall satisfactory fit to all linewidth data indicates that $\sigma_{g\perp}$ decreases with increasing P_b density. Both fitting results can be consistently interpreted within the present understanding of the defect-strain relationship. In this interpretation, defects are created to account for interfacial stress on an atomic scale level, thereby allowing the surrounding interface bonds to relax. As the P_b density in-

creases, the local relaxation should become more global by percolation. The decrease in strain broadening of the linewidth is interpreted as a manifestation of this relaxation. Apparently, maximum relaxation is attained with $[P_b] \sim 3.1 \times 10^{13}\,\mathrm{cm}^{-2}$.

In order to further isolate dipolar and strain broadening effects experimentally, observations on a partially hydrogen passivated sample of maximum P_b site density were compared with an as oxidized specimen, both exhibiting about equal densities of ESR active P_b sites. Though a small change in the ratio of dipolar versus strain broadening contribution is observed, the interpretation of these results is complicated by the previously experimentally observed spread in the activation energy for depassivation and the unknown influence of the incorporation of hydrogen on the interface stress situation.

---

*Electronic address: bert.nouwen@fys.kuleuven.ac.be FAX: +/32-16-327987.

[1] A. Stesmans, Phys. Rev. B **48**, 2418 (1993).

[2] P. J. Caplan, E. H. Poindexter, B. E. Deal and R. R. Razouk, J. Appl. Phys. **50**, 5847 (1979).

[3] K. L. Brower, Appl. Phys. Lett. **43**, 1111 (1983).

[4] N. M. Johnson, D. K. Biegelsen, and M. D. Moyer, J. Vac. Sci. Technol. **19**, 390 (1981); K. L. Brower, Phys. Rev. B **38**, 9657 (1988).

[5] A. Stesmans and V. V. Afanas'ev, Appl. Phys. Lett. **72**, 2271 (1998).

[6] K. L. Brower, *Proceedings of the 13th International Conference on Defects in Semiconductors*, edited by L. C. Kimmerling and J. M. Parsey (The Metallurgical Society of AIME, Warrendale, PA, 1985).

[7] J. H. Van Vleck, Phys. Rev. **74**, 1168 (1948).

[8] K. L. Brower and T. J. Headley, Phys. Rev. B **34**, 3610 (1986).

[9] A. Stesmans and G. Van Gorp, Phys. Rev. B **42**, 3765 (1990).

[10] G. Van Gorp and A. Stesmans, Phys. Rev. B **45**, 4344 (1992).

[11] A. Stesmans and V. V. Afanas'ev, Phys. Rev. B **54**, R11 129 (1996).

[12] K. L. Brower, Phys. Rev. B **33**, 4471 (1986).

[13] A. Stesmans and J. Braet, in *Insulating Films on Semiconductors*, edited by J. J. Simonne and J. Buxo (Amsterdam, North-Holland, 1986), p. 25.

[14] A. Stesmans, Semicond. Sci. Technol. **4**, 1000 (1989).

[15] See, e.g., J. H. Mazur, R. Gronsky and J. Washburn, Proc. Soc. Photo-Opt. Instrum. Eng. **463**, 88 (1984); J. Wollschlager and Henzler, Phys. Rev. B **39**, 6052 (1989); A. Ourmazd, J. A. Rentschler, and J. Bevk, Appl. Phys. Lett. **53**, 743 (1988).

[16] A. Stesmans, Appl. Phys. Lett. **48**, 972 (1986); Z. Phys. Chem. (Leipzig) **151**, 191 (1987).

[17] G. D. Watkins and J. W. Corbet, Phys. Rev. **134**, 1359 (1964).

[18] W. J. C. Grant and M. W. P. Strandberg, Phys. Rev. A **135**, A175 (1964).

[19] G. W. Parker, Am. J. Phys. **38**, 1432 (1970).

[20] D. J. Breed, Ph.D. thesis, University of Amsterdam (1969).

[21] A. Carrington and A. D. McLachlan, *Introduction to Magnetic Resonance* (Harper and Row, New York, 1967), p. 32.

[22] P. M. Richards and M. B. Salamon, Phys. Rev. B **9**, 32 (1974).

[23] C. Kittel and E. Abrahams, Phys. Rev. **90**, 238 (1953).

[24] A. Stesmans, Appl. Phys. Lett. **68**, 2723 (1996); Physica B **273-274**, 1015 (1999).